RESEARCH ARTICLE

Effect of Zinc-doping on the Reduction of the Hot-carrier Cooling Rate in Halide Perovskites

Qi Wei[a,†] Jun Yin,[b, †] Osman M. Bakr,[b] Ze Wang,[c] Chenhao Wang,[c] Omar F. Mohammed,[b,*] Mingjie Li,[c,*] Guichuan Xing[a,*]

[a] Dr. Q. Wei, Prof. G. C. Xing
Joint Key Laboratory of the Ministry of Education, Institute of Applied Physics and Materials Engineering
University of Macau
Macao SAR 999078, China
E-mail: gcxing@um.edu.mo (G. Xing)

[b] Dr. J. Yin, Prof. O. M. Bakr, Prof. O. F. Mohammed
Division of Physical Science and Engineering
King Abdullah University of Science and Technology
Thuwal 23955-6900, Kingdom of Saudi Arabia
E-mail: omar.abdelsaboor@kaust.edu.sa (O. F. Mohammed)

[c] Mr. Z. Wang, Mr. C. C. Wang, Prof. M. J. Li
Department of Applied Physics,
The Hong Kong Polytechnic University
Hung Hom, Kowloon, Hong Kong
E-mail: ming-jie.li@polyu.edu.hk (M. J. Li)

† These authors contributed equally to this work.

Supporting information for this article is given via a link at the end of the document.

Abstract: Fast hot-carrier cooling process in the solar-absorbers fundamentally limits the photon-energy conversion efficiencies. It is highly desirable to develop the solar absorber with long-lived hot-carriers at sun-illumination level, which can be used to develop the hot-carrier solar cells with enhanced efficiency. Herein, we reveal that zinc-doped (0.34%) halide perovskites have the slower hot-carrier cooling compared with the pristine sample through the transient absorption spectroscopy measurements and theoretical calculations. The hot-carrier energy loss rate at the low photoexcitation level of 10^{17} cm^{-3} is found to be ~3 times smaller than that of un-doped perovskites for 500-K hot carriers, and up to ten times when the hot-carrier temperature approaching the lattice temperature. The incorporation of zinc-dopant into perovskites can reduce the nonadiabatic couplings between conduction bands, which retards the photogenerated hot-carriers relaxation process. Our findings present a practical strategy to slow down the hot-carrier cooling in perovskites at low carrier densities, which are valuable for the further development of practical perovskite hot-carrier photovoltaics.

Introduction

Hot carriers are initially generated charge carriers upon the above-band photoexcitation.[1] The fast hot-carrier cooling is one of the major energy losses in the current solar cells.[2] Hot-carrier solar cell that designed for hot carriers collection is considered as a kind of next-generation photovoltaic techniques with photon-energy conversion efficiency beyond the Shockley–Queisser (SQ) limit.[2b] To develop the feasible and practical hot-carrier solar cells, the challenge is to find the solar absorbers from which the slow hot-carrier cooling together with the efficient hot-carrier extraction can be achieved at the low photoexcited carrier densities (i.e., comparable with photoexcitation under AM1.5 illumination). However, the hot-carrier cooling in the conventional semiconductors (e.g., Silicon, InN, GaN and GaAs) occurs very fast (tens of fs at low carrier density),[3] which makes the hot carrier-extraction extremely challenging. Therefore, developing the solar absorbers with slower hot-carrier cooling at the low carrier density is key to achieve the feasible high-efficiency hot-carrier solar cells.[4]

Metal halide perovskites (APbX$_3$, A = Cs$^+$, CH$_3$NH$_3^+$, CH(NH$_2$)$_2^+$, X= I$^-$, Br$^-$ or Cl$^-$) as solar absorbers have attracted much attention in solution-processed solar cells in the past decade. Recently, extensive investigations have been focused on the study of hot-carrier cooling dynamics in halide perovskites (including thin films and nanocrystals) due to the slower hot-carrier cooling lifetime compared with the above mentioned conventional semiconductors.[3d, 4a, 5] The hot-carrier cooling times up to 10^2-10^3 ps have been reported in halide perovskites. However, it should be noted that such achievements were obtained under the high pump fluence with the photoexcited carrier densities of 10^{18} to 10^{19} cm^{-3}.[3d, 6] At the low carrier densities of ~10^{17} cm^{-3}, the hot-carrier cooling lifetime drops down to 10-10^2 fs.[5d, 7] Here, to develop the practical hot-carrier solar cell, the challenge is how to tune the perovskites to further reduce the hot-carrier cooling rate for efficient extraction the high-temperature hot-carriers at low carrier densities (<10^{18} cm^{-3}) in perovskites. Until now, the reported methods to reduce the hot-carrier cooling at the low carrier density mainly include: (1) reducing the sample dimension: slower hot-carrier cooling was observed in smaller perovskite nanocrystals due to quantum confinement effect;[5c, 8] (2) halide or cation tuning in perovskite nanocrystals.[5a, 5d] However, to the best of our knowledge, few studies have tackled this problem to tune the hot carrier lifetime in perovskite thin films.

Doping small amount of metal ions (such as Cu^{2+}, Zn^{2+} and Mn^{2+}, etc) to partially substitute for the lead position in the perovskites has been recently demonstrated to be an effective method to enhance the efficiency and stability of perovskites by reducing the defects/traps and improving the film qualities.[9] As the hot-carrier

cooling at low carrier density is mainly affected by the defects/traps, it is thus of great interest to explore the effect of metal-ions doping on the hot-carrier cooling and extraction dynamics in halide perovskites at low photoexcited carrier densities. And also, few studies have been reported on tuning the hot-carrier cooling dynamics via metal-ion doping in halide perovskites (both thin films or nanocrystals). In this work, we investigated the hot-carrier cooling and extraction dynamics in Zn-doped $CsPbI_2Br$ perovskite films at the low carrier injection level of 10^{17} cm^{-3}. We found that Zn-doping can reduce the defects density as well as the hot-carrier cooling rate obviously. Our transient absorption spectroscopy measurements demonstrated a three-times reduction of 500-K hot-carrier cooling rate in 0.34% Zn-doped perovskite film than un-doped sample, which further enabled the successful hot-carrier extraction at the interface of these doped perovskites. Through the nonadiabatic molecular dynamics calculations, the slow hot carrier relaxation observed in Zn-doped perovskite can be attributed to the reduction of nonadiabatic couplings between conduction bands and introduced additional relaxation channel arising from the Zn dopant. This work provides a new strategy for retarding and utilizing the hot-carriers in halide perovskites for the development of next-generation photovoltaics.

Results and Discussion

The samples in this study are pristine un-doped and Zn-doped $CsPbI_2Br$ (with Zn-doping concentration from 0.34%-2.04%) thin films with a thickness of about 100 nm on quartz substrates. The bandgap of perovskites is not changed at various doping levels (see UV-Vis spectra in Fig. S1). The Zn^{2+} doping in our samples has been verified by XRD and XPS measurements. Zn-doping would induce the lattice constriction of the perovskite structure due to the smaller radius of Zn^{2+} (0.74 Å) than that of Pb^{2+} (1.19 Å). The (200) XRD peak slightly shifts to higher degree in Zn-doped perovskite (Fig. S2), thus suggesting that the Pb^{2+} ions are partially replaced by the smaller Zn^{2+} ions. And also, XPS measurements (Fig. S3) confirmed the state of Zn^{2+} in our doped samples. PL-mapping analysis demonstrates the large-area uniformity of our un-doped and doped film samples (Fig. S4). From our power-dependent PL measurements (Fig. S5), the bulk trap densities are 2.1×10^{16} cm^{-3} and 1.0×10^{16} cm^{-3} for un-doped and Zn-doped samples, respectively, and the surface trap densities of un-doped perovskite is one order of magnitude larger than that of Zn-doped perovskite (3.3×10^{17} cm^{-3} vs 2.7×10^{16} cm^{-3}). The detailed fabrication methods and the other structure characterizations can be found in our previous report.[10]

To investigate the hot-carrier dynamics in $CsPbI_2Br$ thin films, fs transient absorption (TA) spectroscopy measurements are performed on the samples (see the Experimental Section for details of TA measurement). According to the previous studies, the hot-carriers cooling dynamics is governed not only by the intrinsic properties of materials, but also by the initial photoexcited hot carrier densities.[3d, 5e, 5h] The higher hot-carrier density would result in longer the hot-carrier cooling lifetime due to the effects such as hot-phonon bottleneck (at ~10^{18} cm^{-3}), Auger-heating (~10^{18}-10^{19} cm^{-3}),[5h] and state-filling (~10^{19} cm^{-3}).[6] To only investigate the Zn-doping effect on hot-carrier cooling dynamics at low carrier density closing to the sun-illumination situation and prevent the above higher-order effects, the initial excitation carrier

density is controlled in the order of magnitude of 10^{17} cm^{-3} at different pump photon energies.

Figure 1 shows the pseudo-color plots and normalized TA spectra of un-doped and 0.34% Zn-doped $CsPbI_2Br$ thin films after 3.10 eV (400 nm) photoexcitation with initial photoexcited carrier density of ~ 3.56×10^{17} cm^{-3}. The TA spectra under other carrier densities are shown in Fig. S8. For both samples, at early time before ~2 ps, we observe a negative ($\Delta A/A < 0$) photobleaching (PB) peak at the position of band-edge (1.95 eV) associated with a positive ($\Delta A/A > 0$) photoinduced absorption (PIA) feature below 1.95 eV. The PB peak originates from the ground-state bleaching (GSB) because of the state-filling of the carriers at the band edge.[11] The PIA signal below the band-edge was attributed to bandgap renormalization.[5d] As compared with un-doped sample, there are additional obvious high energy tails observed above the band-edge at ~2.0-2.2 eV in the TA spectra of the Zn-doped $CsPbI_2Br$ thin film (Figs. 1c and 1d). The high-energy tails of the TA spectrum originate from the rapid distribution of initial non-equilibrium carriers into a Fermi-Dirac distribution via elastic scatterings (including electron-hole scattering at low pump fluence and carrier–carrier scattering at high pump fluence) that can be characterized by a carrier temperature T_c.
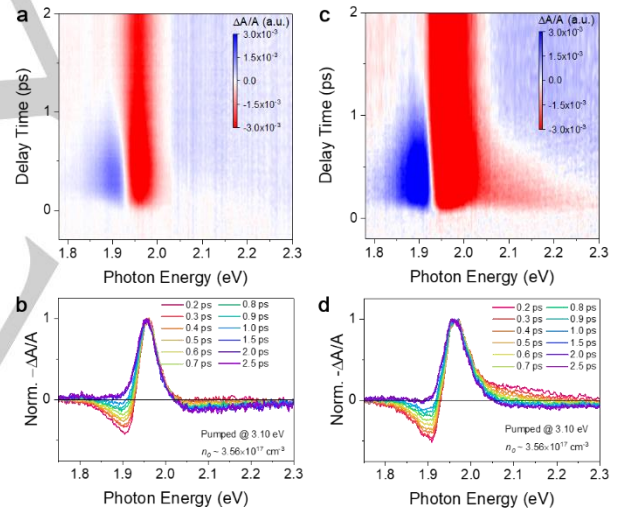

Figure 1. Transient absorption spectra of pristine and Zn-doped $CsPbI_2Br$ ($CsPb_{99.66\%}Zn_{0.34\%}I_2Br$) perovskites. (a) Pseudo colour plot and (b) normalized TA spectra of pristine $CsPbI_2Br$ thin film. (c) Pseudo colour plot and (d) normalized TA spectra for Zn-doped $CsPbI_2Br$ thin film. The photoexcitation energy is 3.10 eV and initial photoexcited carrier density is ~ 3.56×10^{17} cm^{-3}.

These high-energy tails gradually disappear with time, indicating the hot-carrier cooling processes. In principle, as the ΔA is a direct correlation of the electron and hole Fermi distributions, the high energy tail of the TA spectrum can be approximately described by the Maxwell-Boltzmann distribution function.[3d, 5d] The carrier temperature (T_c) can thus be obtained by fitting the high energy tail using the above equation (see Supplementary Note 1 and Figure S6 for fitting procedures and fitted curves). To ensure that the hot carriers have reached a quasi-equilibrium via the carrier-carrier scattering after the initial fs-pulse excitation, the hot-carrier temperatures are analyzed from TA spectra after 0.5 ps time delay. The extracted hot-carrier temperature, energy loss rate and

band-edge PB peak rising dynamics of pristine and Zn doped CsPbI$_2$Br films under photoexcitation of 3.10 eV and 3.54 eV are shown in Fig. 2a-f.

Under 3.10 eV photoexcitation (corresponding to the photoexcited hot-carrier with 1.15 eV excess energy) with carrier density of 3.56×10^{17} cm^{-3}, the extracted carrier temperature is retained at the room temperature for un-doped sample. No hot-carrier distributions (i.e., absence of high energy tail as shown in Fig. 1b) is observed due to the faster hot-carrier cooling than the time-resolution of ~100 fs in our TA measurements. In contrast, for the Zn-doped sample at same carrier density, the initial hot-carrier temperature at 500 fs is ~650 K, and hot-carrier temperature cools down to 500 K (used as a benchmark here) at 0.65 ps (Fig. 2a). Furthermore, the energy loss rate per carrier (J_r) can be obtained from the extracted T_c with -1.5k_bdT_c/dt. As shown in Fig. 2b, J_r decreases slowly from 0.2 to 0.07 eV ps^{-1} until T_c reaches ~ 500 K. Subsequently, J_r declines rapidly as the hot-carrier temperature

approaching the lattice temperature. Such energy loss can be described with the following carrier-phonon interaction processes. At low carrier density, the hot-carrier cooling mechanism is mainly through the carrier-LO phonon interactions, during which the hot carriers lose their excess energies through the dominant Fröhlich interactions via LO phonon emission.[5e, 12] The LO phonon modes will then decay into the daughter acoustic phonon modes via the slow phonon-phonon interactions until the T_c cooling down to the lattice temperature. The energy loss rate reduces suddenly when the T_c is close to the lattice temperature, which is due to the slow thermal equilibration between LO phonons and acoustic phonons. The above processes can be expressed by the following LO–phonon interaction model (see the Supplementary Note 2 and Equation 2 in Supporting Information).[13] The fitted characteristic LO-phonon lifetime τ_{LO} (red curve in Fig. 2b) in Zn-doped sample is 330±10 fs, and the acoustic phonon temperature T_a is 309±5 K.
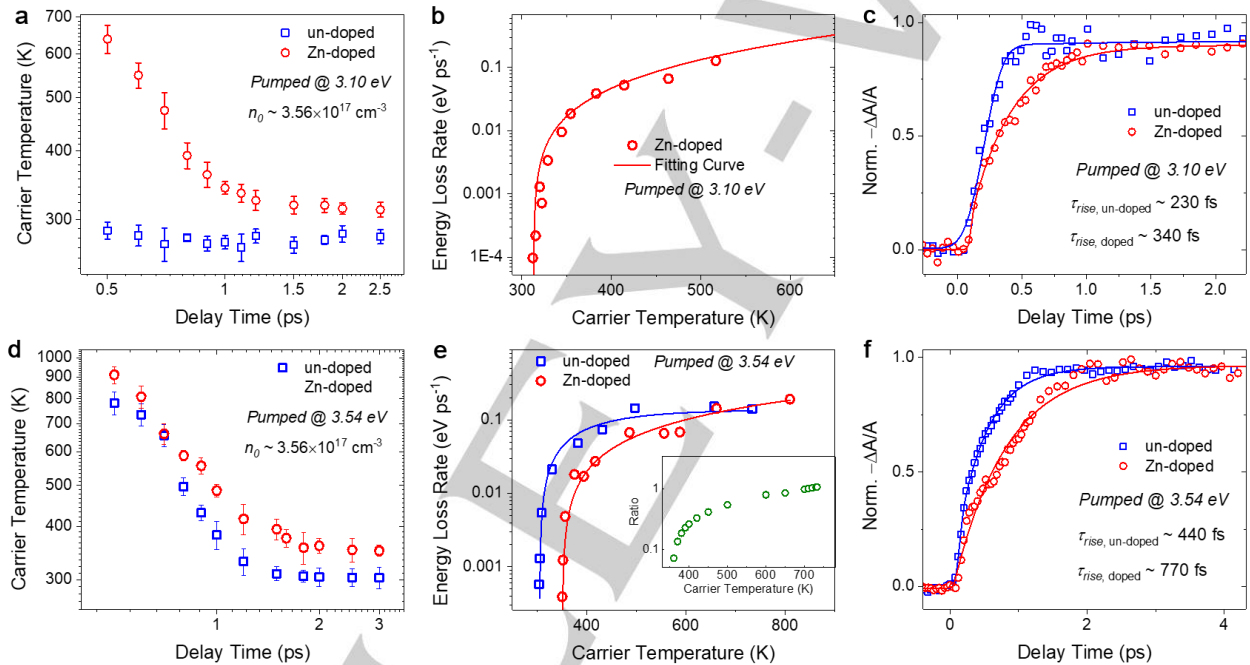

Figure 2. Hot-carrier dynamics analyzation in pristine and Zn-doped CsPbI$_2$Br (CsPb$_{99.66\%}$Zn$_{0.34\%}$I$_2$Br) thin films. (a, d) Average hot-carrier temperatures as a function of the delay time for the un-doped and Zn-doped CsPbI$_2$Br thin films, the average value was calculated from five sets of experimental results. The error bar represents the standard deviation. (b, e) Energy loss rate of hot-carrier as a function of carrier temperature for the un-doped and Zn-doped CsPbI$_2$Br thin films. The solid lines are fittings using LO–phonon interaction model. The inset of Fig. 2e: the energy-loss-rate ratio of the doped over that of un-doped sample at different carrier temperatures. (c, f) Normalized TA dynamics probed at band-edges for un-doped and Zn-doped CsPbI$_2$Br thin films. Photoexcited hot-carrier densities and pump photon energies are 3.56×10^{17} cm^{-3} and 3.10 eV in (a)-(c), and 3.56×10^{17} cm^{-3}, 3.54 eV in (d)-(f), respectively.

The T_a is close to the lattice temperature, indicating the negligible hot-phonon bottleneck effect at such low carrier densities. Except for the time-dependent hot-carrier temperature and energy loss rate, the building up of band-edge PB signal can represent the hot-carrier cooling process from the higher excited energy states to the band-edges. The rise time of band edge PB signal represents the average relaxation time of all photoexcited carriers to the band edge. Figure 2c presents the normalized kinetics probed at band-edge for non-doped and Zn-doped CsPbI$_2$Br thin films. Obviously, the Zn-doped sample has a slower building-up process for PB signal. The rise time (Fig. 2c) of the PB peak is

340 fs for Zn-doped sample vs 230 fs for un-doped one. In order to investigate the cooling dynamics of hot-carriers with higher excess energy, we further studied the hot-carrier dynamics in the samples under photoexcitation energy of 3.54 eV (corresponding to excess energy of ~1.6 eV) with carrier density of 3.56×10^{17} cm^{-3}. Under higher-energy photoexcitation, the high-energy tails of TA spectra are observed in un-doped sample (Fig. S6). Figure 2d shows the extracted hot-carrier temperatures as a function of delay time. The higher excess energy gained by the hot-carrier will lead to a larger population build-up of non-equilibrium LO phonons, thus, the hot-carrier temperature and the decay time of

hot-carrier temperature become higher and longer as compared with the results in Fig. 2a. Figure 2e shows the extracted carrier-temperature dependent J_r, from which the fitted τ_{LO} are 260±10 fs and 330±10 fs for un-doped and Zn-doped samples, respectively. The inset of Fig. 2e shows the energy-loss-rate ratio of the doped and un-doped sample at different carrier temperatures. The energy loss rate J_r of 500-K hot carriers in Zn-doped sample is ~2 times slower than that of un-doped sample. When the carrier temperature approaches lattice temperature, J_r of the doped sample decreases down to ~one tenth of that of un-doped sample. Furthermore, as shown in Fig. 2f, τ_{peak} of PB increases from 440 fs to 770 fs after Zn-doping (75% increment). The above results clearly indicate that Zn-doping in perovskite can effectively slow down the hot-carrier cooling and reduce the energy loss rate.

Furthermore, the hot carrier dynamics at higher carrier densities are also performed on pristine and Zn-doped samples (see carrier density dependent TA spectra and extracted hot-carrier temperature dynamics in Fig. S7-S9 and Fig. 3). By increasing photoexcited carrier density to 5.34×10^{17} cm^{-3}, the high energy tail appears in un-doped sample (see TA spectra in Fig. S5) with the initial hot-carrier temperature of ~310 K at 500 fs (Fig. 3). In comparison, after Zn-doping, the initial hot-carrier temperature increases to ~710 K, and PB rise time increases from 280 fs to 540 fs (~80% increment, see Fig. 3b).

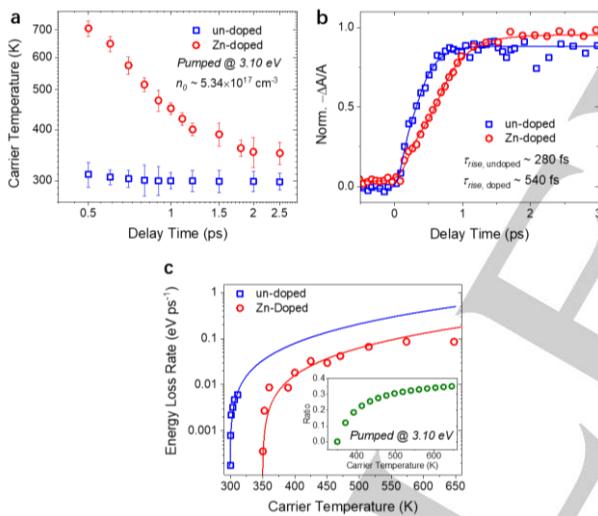**Figure 3. Hot-carrier dynamics analyzation in pristine and Zn-doped CsPbI₂Br (CsPb$_{99.66\%}$Zn$_{0.34\%}$I₂Br) thin films.** (a) Hot-carrier temperatures as a function of the delay time for the un-doped and Zn-doped CsPbI₂Br thin films. (b) Normalized TA dynamics probed at the band-edges for the un-doped and Zn-doped CsPbI₂Br thin films. Photoexcited hot-carrier density and pump photon energies are 5.34×10^{17} cm^{-3} and 3.10 eV, respectively. (c) Energy loss rate as a function of carrier temperature for the un-doped and Zn-doped CsPbI₂Br thin films. The solid lines are fittings using LO–phonon interaction model.

The energy loss rate J_r of 500-K hot carriers in Zn-doped sample reduces further down to ~3 times slower than that of un-doped sample (Fig. 3c inset). The fast hot-carrier cooling in the pristine sample is reflected by the faster τ_{LO} of 240±10 fs as compared to 480±10 fs for Zn doped sample under the same carrier density (LO-phonon lifetimes are fitted by Eq.2 shown in Fig. 3c). The possible reason for the absence of high energy tail in un-doped sample is that the most of the injected hot carriers are trapped by

defects at very low carrier density before they form a Fermi-Dirac distribution, which thus induces the unnoticeable hot carrier effect from TA measurement. Besides, it should be pointed out that at such a higher carrier density of 5.34×10^{17} cm^{-3}, the hot-phonon bottleneck effect starts to appear in Zn-doped sample. The fitted curve of the energy loss rates (red curve in Fig. 3c) by using Eq. 2 produces an acoustic phonon temperature T_a of ~348 K. The higher T_a indicates the existence of the hot phonon bottleneck effect, i.e., the reduced decay of LO phonons caused by large non-equilibrium LO phonon population due to the partial heating of acoustic modes.

However, for the un-doped sample, even when the photoinduced carrier density reaches ~ 7.12×10^{17} cm^{-3} under 3.1-eV excitation, the extracted T_a is still near the lattice temperature (Fig. S9), which indicates that the hot-phonon bottleneck effect is not as strong as Zn-doped perovskites at similar carrier densities. The main reason for the ineffective hot-phonon bottleneck effect should be the fast hot-carrier cooling which gives the fast LO-phonon lifetime in the un-doped sample. Since the slower hot carrier cooling via the longer LO phonon decay is required to enhance the non-equilibrium LO phonon populations given that hot-carrier cooling is a cascade process between electron–LO phonon and anharmonic phonon–phonon interactions.[5h]

To verify that if the slower hot-carrier cooling can be obtained with higher Zn-doping concentrations in perovskites, two more examples are measured by TA with same pump conditions. However, when the Zn-doping concentrations increases further to 0.68% and 2.04%, the hot-carrier cooling lifetime decreases (Fig. S11). This reduction should due to the fact that the higher-doping degrades the sample quality as revealed by the emergence of many pinholes in the films (see SEM images in Fig. S12), which may be correlated with the limited solid solubility of Zn in CsPbI₂Br precursor solution and large amounts of defects acting as the traps for hot carriers with increasing Zn-doping. Therefore, a proper amount of Zn-doping without affecting the perovskite quality is essential and key to slow down the hot-carrier cooling.

To understand the mechanism of Zn-doping effect on the hot-carrier cooling dynamics observed in the CsPbI₂Br thin film, we performed nonadiabatic molecular dynamics (NAMD) calculations on the model system, 2×2×2 CsPbI₃ and CsPbBr₃ supercell, without and with Zn dopant (i.e., a Pb^{2+} ion is replaced by a Zn^{2+} ion) using the fewest-switches surface hopping (FSSH) method.[14] The spin-orbit coupling (SOC) effects was considered in our NAMD calculations as relativistic effects which are expected to accelerate the intra-band relaxation processes between conduction bands of perovskite systems.[5b, 15] Although including SOC decreases the band gaps by ~0.9 eV (see the comparisons between Figs. 4a, b and Fig. S13 for CsPbI₃ and between Figs. S17a, b and S14), it would not affect our NAMD analysis on the hot-carrier relaxation between conduction bands as the initial state was evaluated by the excess energy above the conduction band minimum (CBM). In addition, our NAMD calculations are not sensitive to the size of the supercells since i) the Zn^{2+} dopant does not induce significant lattice distortions once it replaces a Pb^{2+} ion and ii) the Zn^{2+} dopant gives the middle-level state at symmetric R-point instead of Γ-point.

When SOC effects are considered, the electrons in pristine CsPbI₃ undergo a fast relaxation from the CBM+3 (i.e., 1.55 eV above the CBM) to CBM, and the population of electrons from the initial state rapidly decays within 100 fs (Figure 4e) because the direct population transfer is most likely to occur between CBM+3

and CBM with a large nonadiabatic coupling (149.9 meV, Figure S14). However, for the Zn-doped case, the hot electrons take a longer time to cool down from the initial CBM+3 (*i.e.*, 1.44 eV above the CBM) to the CBM+1 and then decays to CBM within 500 fs (Figure 4f) due to the reduced nonadiabatic coupling between CBM+3 and CBM (17.5 meV) and between CBM+1 and CBM (50.1 meV). The similar electron relaxation processes in $CsPbBr_3$ without and with a Zn dopant can be drawn that the hot electrons take a longer time to cool down from the initial CBM+2 to CBM (see the NAMD results in Figures S16 and S17). Our calculated hot electron relaxation time including SOC is consistent well with the experimental values derived from the femtosecond TA measurements. The nonadiabatic couplings between the high-energy conduction bands in pristine $CsPbBr_3$ are significantly larger than those in Zn-doped $CsPbBr_3$. Therefore, the fast hot-electron relaxation among the conduction bands in pristine $CsPbI_3$ or $CsPbBr_3$ is due to the larger nonadiabatic coupling induced by the overlapping of the electronic charge density between these conduction bands involved in the excited electron relaxations (Figures 4b, d). In addition, the Zn^{2+} dopant introduced a new localized state at R-point of the Brillouin zone in $CsPbBr_3$ (*i.e.*, below CBM+2 at Γ-point and slightly above the CBM+1 at Γ-point) and in $CsPbI_3$ (*i.e.*, slightly below the CBM at Γ-point). Therefore, such new state near CBM in the mixed perovskite $CsPbI_2Br$ after Zn-doping could become another channel for slowing down the hot-carrier cooling. Furthermore, as mentioned above for Fig. 3, the slower hot-carrier cooling via carrier phonon interaction can induce the more efficient hot-phonon bottleneck effect, which thus account for the easier observation of hot-phonon bottleneck and even slower cooling lifetime at higher carrier densities in Zn-doped sample.

Slower hot-carrier cooling in the Zn-doped perovskite can result in the longer hot-carrier diffusion length, which improves the possibility of the hot-carrier extraction at the interface of perovskite/extraction layer. Using the estimated hot-carrier diffusion coefficient D_{hot} of 20.67 cm^2 s^{-1}, and 500-K hot-carrier lifetime of 0.65 ps (at carrier density 3.56×10^{17} cm^{-3}, see Figure S18 and Supplementary Note 3 for details), we estimated the hot-carrier diffusion length L_{hot} of ~ 36 nm, which reveal that it is technically feasible to extract the hot carriers from thin perovskite films. We then investigated the possibility of hot-electron/-hole extractions from perovskite films by using the electron/hole transportation layers, respectively. After adding the charge extraction layer, the PB peak and the high-energy tail intensities reduced and the initial hot-carrier temperature drops from ~ 700 K to 379 K and 391 K within 0.5 ps in perovskite/PTAA (electron transport layer) and perovskite/SnO_2 (hole transport layer) bilayers, respectively (Fig. S18). Similar phenomena were observed in $MAPbBr_3$ NCs films and $MAPbI_3$ films,[5c, 16] which were claimed to be due to the hot-carrier extraction. However, [l]considering that other possible hot-carrier trapping channels (such as interfacial defects, strains) may be exist after adding new material on the surface of perovskites film, more detailed experiments are required to prove the hot-carrier are truly extracted in the extraction layers, which should be investigated especially by combining the electrical measurements in the future.
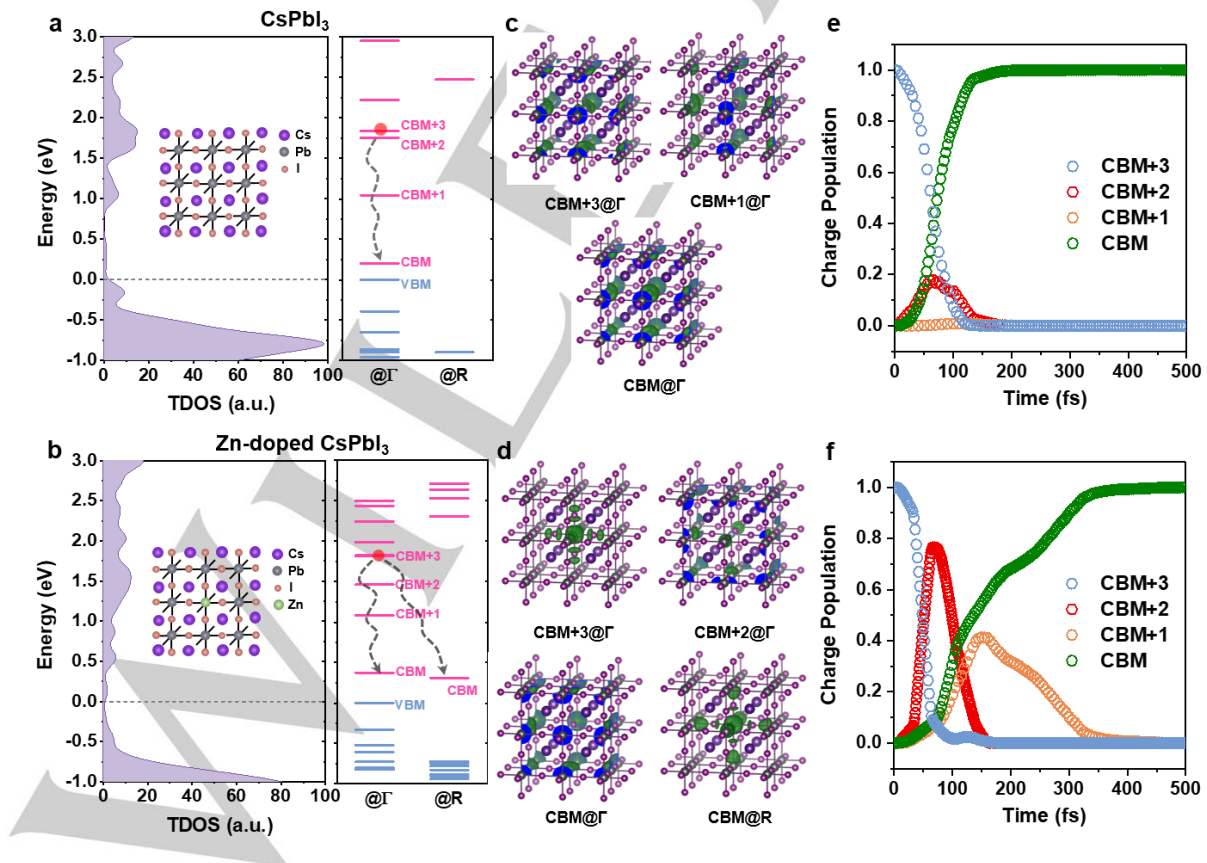

Figure 4. Nonadiabatic molecular dynamics calculations. (a, b) Calculated total density of states (TDOS) and energy levels, (c, d) electronic charge densities for CBM+3, CBM+2, CBM+1, and CBM at the Γ-point as well as CBM at the R-point, and (e, f) time evolution of hot electron relaxation starting from CBM+3 for

pristine CsPbI3 supercell and Zn-doped CsPbI$_3$ supercell (the VBM is set to zero energy). All calculations were performed at the GGA/PBE level with spin-orbit coupling (SOC).

Conclusion

In summary, our femtosecond TA spectroscopy measurements reveal that the hot-carrier cooling relaxation in all-inorganic lead-halide perovskites is obviously prolonged via proper Zn-doping. The hot-carrier energy loss rate can be reduced down to three times slower than that of un-doped perovskites for 500-K hot carriers at low carrier injection level. In consistent with measurements, the NAMD calculations proved that the introduced Zn^{2+} dopant can create a new delocalized state at R-point of the Brillouin zone which may become a channel for slowing down the hot electron relaxation. Our findings not only provide a strategy to prolong the hot-carrier cooling time in halide perovskite via Zn-doping, but also demonstrate the possibility to utilize the hot-carriers for the development of high-efficiency optoelectronics.

Acknowledgements

Keywords: Halide perovskites • Hot-carrier cooling • Doped perovskites • Nonadiabatic molecular dynamics • Carrier extraction.

[1]   W. A. Tisdale, K. J. Williams, B. A. Timp, D. J. Norris, E. S. Aydil, X.-Y. Zhu, *Science* **2010**, 328, 1543-1547.
[2]   a) A. J. Nozik, *Annu. Rev. Phys. Chem.* **2001**, 52, 193-231; b) R. T. Ross, A. J. Nozik, *J. Appl. Phys.* **1982**, 53, 3813-3818.
[3]   a) Y.-C. Wen, C.-Y. Chen, C.-H. Shen, S. Gwo, C.-K. Sun, *Appl. Phys. Lett.* **2006**, 89, 232114; b) Z. Vardeny, J. Tauc, *Phys. Rev. Lett.* **1981**, 46, 1223-1226; c) D. J. Suntrup III, G. Gupta, H. Li, S. Keller, U. K. Mishra, *Appl. Phys. Lett.* **2014**, 105, 263506; d) Y. Yang, D. P. Ostrowski, R. M. France, K. Zhu, J. Van De Lagemaat, J. M. Luther, M. C. Beard, *Nat. Photon.* **2016**, 10, 53–59.
[4]   a) M. Li, J. Fu, Q. Xu, T. C. Sum, *Adv. Mater.* **2019**, 1802486; b) S. Kahmann, M. A. Loi, *J. Mater. Chem. C* **2019**, 7, 2471-2486.
[5]   a) J. Chen, M. E. Messing, K. Zheng, T. Pullerits, *J. Am. Chem. Soc.* **2019**, 141, 3532-3540; b) J. Yin, P. Maity, R. Naphade, B. Cheng, J.-H. He, O. M. Bakr, J.-L. Brédas, O. F. Mohammed, *ACS Nano* **2019**, 13, 12621-12629; c) M. Li, S. Bhaumik, T. W. Goh, M. S. Kumar, N. Yantara, M. Grätzel, S. Mhaisalkar, N. Mathews, T. C. Sum, *Nat. Commun.* **2017**, 8, 14350; d) M. B. Price, J. Butkus, T. C. Jellicoe, A. Sadhanala, A. Briane, J. E. Halpert, K. Broch, J. M. Hodgkiss, R. H. Friend, F. Deschler, *Nat. Commun.* **2015**, 6, 8420; e) J. Yang, X. Wen, H. Xia, R. Sheng, Q. Ma, J. Kim, P. Tapping, T. Harada, T. W. Kee, F. Huang, *Nat. Commun.* **2017**, 8, 14120; f) H. Chung, S. I. Jung, H. J. Kim, W. Cha, E. Sim, D. Kim, W. K. Koh, J. Kim, *Angew. Chem. Int. Ed.* **2017**, 56, 4160-4164; g) T. R. Hopper, A. Gorodetsky, A. Jeong, F. Krieg, M. I. Bodnarchuk, M. Maimaris, M. Chaplain, T. J. Macdonald, X. Huang, R. Lovrincic, M. V. Kovalenko, A. A. Bakulin, *Nano Lett.* **2020**, 20, 2271-2278; h) J. Fu, Q. Xu, G. Han, B. Wu, C. H. A. Huan, M. L. Leek, T. C. Sum, *Nat. Commun.* **2017**, 8, 1300; i) H. Zhu, K. Miyata, Y. Fu, J. Wang, P. P. Joshi, D. Niesner, K. W. Williams, S. Jin, X.-Y. J. S. Zhu, *Science* **2016**, 353, 1409-1413.
[6]   H.-H. Fang, S. Adjokatse, S. Shao, J. Even, M. A. Loi, *Nat. Commun.* **2018**, 9, 243.
[7]   J. M. Richter, F. Branchi, F. Valduga de Almeida Camargo, B. Zhao, R. H. Friend, G. Cerullo, F. Deschler, *Nat. Commun.* **2017**, 8, 376.
[8]   B. Yu, L. Chen, Z. Qu, C. Zhang, Z. Qin, X. Wang, M. Xiao, *J. Phys. Chem. Lett.* **2020**, DOI: 10.1021/acs.jpclett.0c03350238-244.
[9]   a) W. Xiang, Z. Wang, D. J. Kubicki, W. Tress, J. Luo, D. Prochowicz, S. Akin, L. Emsley, J. Zhou, G. Dietler, *Joule* **2019**, 3, 205-214; b) L. Chen, L. Wan, X. Li, W. Zhang, S. Fu, Y. Wang, S. Li, H.-Q. Wang, W. Song, J. Fang, *Chem. Mater.* **2019**, 31, 9032-9039; c) C. F. J. Lau, M. Zhang, X. Deng, J. Zheng, J. Bing, Q. Ma, J. Kim, L. Hu, M. A. Green, S. Huang, *ACS Energy Lett.* **2017**, 2, 2319-2325; d) Q. Wei, M. Li, Z. Zhang, J. Guo, G. Xing, T. C. Sum, W. Huang, *Nano Energy* **2018**, 51, 704-710; e) N. Mondal, A. De, A. Samanta, *ACS Energy Lett.* **2019**, 4, 32-39; f) X. Shen, Y. Zhang, S. V. Kershaw, T. Li, C. Wang, X. Zhang, W. Wang, D. Li, Y. Wang, M. Lu, L. Zhang, C. Sun, D. Zhao, G. Qin, X. Bai, W. W. Yu, A. L. Rogach, *Nano Lett.* **2019**, 19, 1552–1559; g) S. S. Mali, J. V. Patil, C. K. Hong, *Adv. Energy Mater.* **2020**, 10, 1902708; h) Q. Xu, K. Meng, Z. Liu, X. Wang, Y. Hu, Z. Qiao, S. Li, L. Cheng, G. Chen, *Adv. Mater. Interfaces* **2019**, 6, 1901259; i) Z.-J. Yong, S.-Q. Guo, J.-P. Ma, J.-Y. Zhang, Z.-Y. Li, Y.-M. Chen, B.-B. Zhang, Y. Zhou, J. Shu, J.-L. Gu, L.-R. Zheng, O. M. Bakr, H.-T. Sun, *J. Am. Chem. Soc.* **2018**, 140, 9942-9951.
[10]   Z. Wang, J. Gan, X. Liu, H. Shi, Q. Wei, Q. Zeng, L. Qiao, Y. Zheng, *J. Power Sources* **2020**, 454, 227913.
[11]   J. S. Manser, P. V. Kamat, *Nat. Photon.* **2014**, 8, 737.
[12]   H. Kawai, G. Giorgi, A. Marini, K. Yamashita, *Nano Lett.* **2015**, 15, 3103-3108.
[13]   V. Klimov, P. H. Bolivar, H. Kurz, *Phys. Rev. B* **1995**, 52, 4728.
[14]   a) A. V. Akimov, O. V. Prezhdo, *J. Chem. Theiry Comput.* **2013**, 9, 4959-4972; b) A. V. Akimov, O. V. Prezhdo, *J. Chem. Theiry Comput.* **2014**, 10, 789-804.
[15]   W. Li, L. Zhou, O. V. Prezhdo, A. V. Akimov, *ACS Energy Lett.* **2018**, 3, 2159-2166.
[16]   I. Dursun, P. Maity, J. Yin, B. Turedi, A. A. Zhumekenov, K. J. Lee, O. F. Mohammed, O. M. Bakr, *Adv. Energy Mater.* **2019**, 9, 1900084.

Entry for the Table of Contents
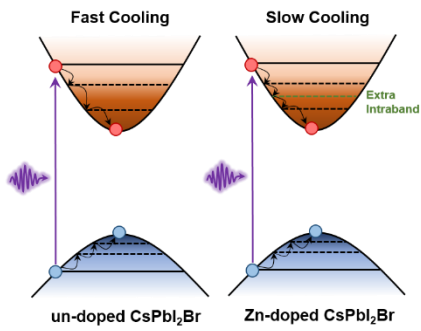
Proper Zn-doping (0.34%) in perovskites is found to be able to significantly slowdown the hot-carrier cooling, the cooling rate of the 500-K hot-carriers can be reduced down to one third of the un-doped sample. Nonadiabatic molecular dynamics calculations uncover the mechanisms of such efficient retardation of the hot-carrier cooling via Zn-doping.